Transport Properties for Turbulent Dispersion from Wall Sources

Bojan M. Mitrovic and Dimitrios V. Papavassiliou
School of Chemical Engineering and Materials Science, The University of Oklahoma, Norman, OK 73019

The dispersion of a passive contaminant by turbulence is not only intrinsically interesting, but also is fundamental to practical heat- and mass-transfer problems. The mechanism of turbulent dispersion from the wall and effects of the molecular Prandtl number are examined. Transport properties for scalar dispersion from an instantaneous line source at the wall of a parallel-plate channel in which fully developed turbulent flow occurs, as well as from a continuous line source, are studied. Numerical experiments using a direct numerical simulation (DNS) of the flow, combined with Lagrangian scalar tracking (LST) of trajectories of thermal markers in the flow field, are conducted. The method is applied for a wide range of molecular Prandtl (Pr) or Schmidt (Sc) number fluids ($0.1 \leq Pr \leq 50{,}000$, which corresponds to liquid metals, gases, refrigerants, lubricants and electrochemical fluids). Results from the DNS/LST method are compared with experimental data, which are available for low Pr or Sc fluids. The turbulent diffusivity and turbulent Prandtl number for the plume that results from a line source are calculated, and an appropriate scaling is proposed. Finally, a model is developed for the prediction of the mean temperature or mean concentration profile as a function of Pr or Sc.

Introduction

Turbulent dispersion is one of the defining characteristics of turbulence and its most important feature so far as industrial and environmental applications are concerned. Accurate modeling and understanding of turbulent scalar transport plays a crucial role in many chemical engineering applications (such as heat exchange, mixing, flows in reactors and catalyst regeneration units, dispersion of pollutants in the atmosphere or in riverbeds). Current engineering approaches involve models that utilize eddy diffusivities, mixing lengths, the turbulent kinetic energy, and/or the rate of turbulence dissipation. These Eulerian models predict the heat-transfer coefficient and the temperature distribution using some form of the Reynolds analogy, which assumes that the eddy diffusivity of heat or mass is directly proportional to the eddy viscosity. They also have to incorporate a considerable degree of empiricism, in the form of variables that need to be calibrated, and they often lead to inaccuracies (Churchill, 1996, 1997).

The development of direct numerical simulations (DNS) of turbulent flows and of turbulent scalar transport removed empiricism and approximation from the calculation of the flow and temperature fields. Such simulations offer the possibility to study the fundamental phenomena that govern turbulent transport (Kasagi and Shikazono, 1995; Moin and Mahesh, 1998). However, due to computational requirements, DNS have been limited to relatively low Reynolds numbers, primarily to parallel-plate channels or unconfined flows, and to a narrow range of fluids with Prandtl number, *Pr*, or Schmidt number, *Sc*, between 0.025 and 10 (Kim and Moin, 1989; Lyons et al., 1991a; Kasagi et al., 1992; Kawamura et al., 1998; Na et al., 1999; Tiselj et al., 2001). It is known that in order to resolve all the scales for the temperature fluctuations in 3-D, the numerical grid has to increase with $Pr^{3/2}$ (Tennekes and Lumley, 1972). Papavassiliou and Hanratty (1995) used Lagrangian methods in conjunction with DNS to study heat transfer for higher *Pr* fluids by orders of magnitude (up to $Pr = 2400$). In the Lagrangian framework, the system of reference moves with the fluid particles, or with the heat/mass markers in the case of turbulent heat/mass transport. The Lagrangian approach, although very difficult to pursue experimentally, is the most natural way of investigating the mechanism of turbulent heat or mass transport, and it can provide significant physical insights. Eulerian results that

Correspondence concerning this article should be addressed to D. V. Papavassiliou.

raise concerns for the application of turbulent transport models (that is, the spatial variation of eddy transport coefficients, the effect of *Pr* on turbulent transport, the dependence of the turbulent *Pr* on the distance from the wall) can be interpreted through Lagrangian reasoning (Eckelman and Hanratty, 1972; Papavassiliou and Hanratty, 1997). The fundamental Lagrangian argument is that the behavior of a heated plane can be synthesized from the behavior of a single, instantaneous, point source located on the plane, and that understanding this behavior leads to an improved understanding of turbulent transport from the wall (Hanratty, 1956).

In order to apply the Lagrangian approach, information must be calculated and gathered along the trajectories of these markers. We will refer to the numerical implementation of this methodology as the Lagrangian scalar tracking (LST) method. In addition to describing heat/mass transfer in a wide range of *Pr* or *Sc*, the LST technique has the advantage that a single computation can be used to reconstruct the behavior in different problem configurations; for example, isothermal and isoflux walls, step change in wall temperature or heat flux, continuous and instantaneous line-source behavior. The contributions of the present article can be summarized as (a) interpretation of the *Pr* effect on turbulent transport from wall sources, (b) development of a model that describes the temperature profile that results from a line source as a function of *Pr*, (c) discussion of the Lagrangian similarity theory in a turbulent shear flow and calculation of Batchelor's universal constant, and (d) extension and validation of LST as a method for obtaining Eulerian quantitative results.

Background

In the Lagrangian approach, the dispersion process is viewed as the result of the random wandering of the fluid particles. The dispersion of a particle from a point source can be described in terms of the mean-squared displacement from the source, $\overline{X^2}$. Einstein (1905) developed the following relation for molecular dispersion in a nonturbulent field

$$\frac{d\overline{X^2}}{dt} = 2D \tag{1}$$

where D is the molecular diffusivity.

The most influential contribution to the theory of turbulent diffusion is Taylor's (1921) description of the dispersion of fluid particles from a point source in homogeneous, isotropic turbulence

$$\frac{d\overline{X^2}}{dt} = 2\overline{u^2}\int_0^t R^L(\tau)\, d\tau \tag{2}$$

where $\overline{u^2}$ is the mean square of the x component of the velocity of the fluid particles and R^L is the Lagrangian correlation coefficient. Saffman (1960) developed an analogous relation for dispersion in the case of heat or mass markers by defining a material autocorrelation function, which differs from the Lagrangian correlation in that it correlates fluid velocity components along the trajectories of markers instead of fluid particles. The markers can move off of a fluid particle as a result of molecular diffusion. Hanratty (1956) used Taylor's theory to describe the transfer of heat across a channel in turbulent flow. An infinite number of line sources of heat along one wall were used to describe the hot plane, and an infinite number of line sinks of heat along the other wall described the behavior of the cold plane. This analysis assumed a homogeneous and isotropic velocity field. Information about the behavior of such wall sources in anisotropic velocity fields is needed in order to use Lagrangian methods to describe Eulerian temperature fields in other, more realistic situations. There are such investigations in the literature, including the work of Poreh and Cermak (1964), Poreh and Hsu (1971), Fackrell and Robins (1982), Shlien and Corrsin (1976), Raupach and Legg (1983), and Incropera et al. (1986), who have carried out experimental studies of wall sources. However, none of these studies give the space-time behavior of an instantaneous source, and only the study of Incropera et al. examines transport in a fully developed channel flow.

Methodology

Details regarding the LST methodology can be found elsewhere (Papavassiliou and Hanratty, 1995, 1997; Ponoth and McLaughlin, 2000; Papavassiliou, 2002a,b; Mito and Hanratty, 2001). However, since LST is not a mainstream approach, this section briefly presents information that is necessary to facilitate the discussion of the results.

In order to calculate trajectories of individual heat or mass markers, detailed instantaneous information about the turbulent field is required. A DNS of fully developed turbulent flow in a channel gives the evolution of the fluctuating Eulerian velocity field at a large number of spatial locations by solving the 3-D, time-dependent Navier–Stokes equations. The validation of the particular DNS code used in this work can be found in previous publications (Lyons et al., 1991b; Guenther et al., 1998). The flow, which is driven by a constant mean pressure gradient, is for an incompressible Newtonian fluid with constant physical properties. The Reynolds number, *Re*, defined with the center-line mean velocity and half-height of the channel, h, is 2660. The simulation is done on a $128\times65\times128$ grid in x, y, z. The streamwise direction is x, the spanwise is z, and the direction normal to the channel is y. The dimensions of the computational box are $4\pi h \times 2h \times 2\pi h$, where $h = 150$ is the half height of the channel in wall units. The flow is regarded as periodic in the streamwise and spanwise directions, with the periodicity lengths λ_x and λ_z, equal to the dimensions of the computational box in these directions. (All variables in this article are made dimensionless with the viscous wall parameters.)

The behavior of a wall source is determined by following the paths of a large number of scalar markers in the flow field created by the DNS. A tracking algorithm (Kontomaris et al., 1993) is used to monitor the trajectories of the markers in space and in time. The motion of the heat markers is decomposed into a convective part and a diffusive part, which depends on *Pr*. The convective part can be calculated from the fluid velocity at the marker position. The equation of

Table 1. Performed Tracking Experiments

Run		Pr	No. of Markers	Simul. Time (t)	Comput. Time
A	a	100	16,129	2,750	Convex C-3 C3880 600 SU
	b	10			
	c	1			
	d	0.1			
B	a	0.7	16,129	2,750	Convex C-3 C3880 600 SU
	b	3			
	c	500			
	d	2,400			
	e	1			
C	a	200	16,129	13,000	HP/convex Exemplar SPP-2000 1050 SU
	b	2,400			
	c	7,000			
	d	15,000			
	e	50,000			
D	a	0.1	145,161	1,600	SGI/CRAY Origin 2000 1180 SU
	b	0.7			
	c	3			
	d	10			
E	a	0.1	145,161	4,000	SGI/CRAY Origin 2000 3390 SU
	b	0.7			
	c	6			
	d	10			
	e	100			

Note: The computational time is given in service units (SU), which are roughly equivalent to CPU hours.

marker motion then is

$$\boldsymbol{V}(\boldsymbol{x}_o,t) = \frac{\partial \boldsymbol{X}(\boldsymbol{x}_o,t)}{\partial t} \tag{3}$$

where $\boldsymbol{V}(\boldsymbol{x}_o,t)$ is the Lagrangian velocity of a marker that is released at location $\boldsymbol{x}_o$, given as $\boldsymbol{V}(\boldsymbol{x}_o,t) = \boldsymbol{U}[\boldsymbol{X}(\boldsymbol{x}_o,t),t]$, where $\boldsymbol{U}$ is the Eulerian velocity of the fluid at the location of the marker at time t. The effect of molecular diffusion is simulated by imposing a 3-D random walk on the particle motion; it is added to the convective part of the motion after each time step, Δt, and takes values from a normal distribution with a zero mean and with a standard deviation, $\sigma = \sqrt{2\Delta t/Pr}$, in wall units. This follows from Einstein's theory for Brownian motion (Eq. 1). The presence of these markers does not affect the flow field, so the behavior of a passive scalar is simulated. (In this article, the scalar quantity is mostly referred to as the temperature, and the dimensionless number as the Prandtl number. The results can be applied to the case of turbulent mass transfer by replacing temperature with concentration and Prandtl number with Schmidt number.)

Five sets of tracking experiments were conducted, as presented in Table 1. The typical procedure was to follow markers for four or five different values of Pr using the same hydrodynamic field. In each of the first three runs a total of 16,129 markers were released instantaneously from a uniform 127×127 rectangular grid that covered the bottom wall of the channel. Runs A and B tracked markers for different values of Pr up to time $t = 2750$, while run C, which corresponds to high-Pr fluids, tracked markers up to time $t =$ 13,000. The velocities and positions of these markers were stored every wall time unit for statistical postprocessing. Runs D and E were conducted by following a total of 145,161 instantaneously released markers in order to estimate the statistical variation of the results and to assess the effect of the number of markers on the statistics. Run D tracked markers for $Pr = 0.1$, 0.7, 3, and 10 up to $t = 1{,}600$, and run E tracked markers for $Pr = 0.1$, 0.7, 6, 10, and 100 up to $t = 4{,}000$. The computations were run on the National Center for Supercomputing Applications (NCSA) computers. The required computational time depended on the number of markers and on the type of supercomputer used; it is shown in Table 1. The time step in all the simulations was $\Delta t = 0.25$.

The building block for the Lagrangian formulation is the probability function $P_1(x - x_o, y, t - t_o | t_o, x_o)$, which represents the joint and conditional probability density function for a marker to be at a location (x, y) at time t, given that the marker was released at x_o at time t_o. This probability can be interpreted physically as concentration (Cermak, 1963), and, thus, as a snapshot of a cloud of contaminants released instantaneously from $x_o = 0$. Probability P_1 can be used to extract information about the behavior of a continuous line source at x_o by integrating over time

$$P_2(x - x_o, y | t_o, x_o) = \int_{t_o}^{\infty} P_1(x - x_o, y, t - t_o | t_o, x_o)\, dt \tag{4}$$

The probability P_2 is calculated for each Pr using a grid that covers the flow domain and counting the number of markers that are present in each grid cell (Papavassiliou, 2002b). The grid in the normal direction is constructed either by dividing the width of the channel uniformly into 300 bins (when $Pr \leq 100$), or by using Chebyshev collocation points to generate 200 bins (when $Pr > 100$) in order to increase the resolution closer to the wall. In the streamwise direction, the grid is stretched, in order to take measurements at long distances downstream from the source. The stretching in the streamwise direction followed the relation $\Delta x_n = 1.06^n \Delta x_{(n-1)}$ with $\Delta x_0 = 5$ in wall units.

Results

Effect of sample size and comparison with experimental data

The numerical error for the LST methodology includes an error associated with the number of markers considered, apart from the usual error due to discretization. Previous work (Papavassiliou and Hanratty, 1997; Papavassiliou, 2002a,b) utilized databases with 16,129 markers and addressed this issue by examining the statistics of the marker trajectories by repeating the calculations with half the markers. That work has shown that results of acceptable accuracy can be obtained with that sample size (16,129 markers), but it was not possible to investigate the effect of sample size further. In the current work, runs D and E involve marker samples that are almost one order of magnitude larger. Figure 1a presents the mean displacement of the markers in the normal direction with time for different sample size. Physically, this is the trajectory of the centroid of a cloud of markers released from an instantaneous line source located at the wall of the channel. At large times, it is expected that the cloud will be uniformly distributed over the width of the channel and the cen-

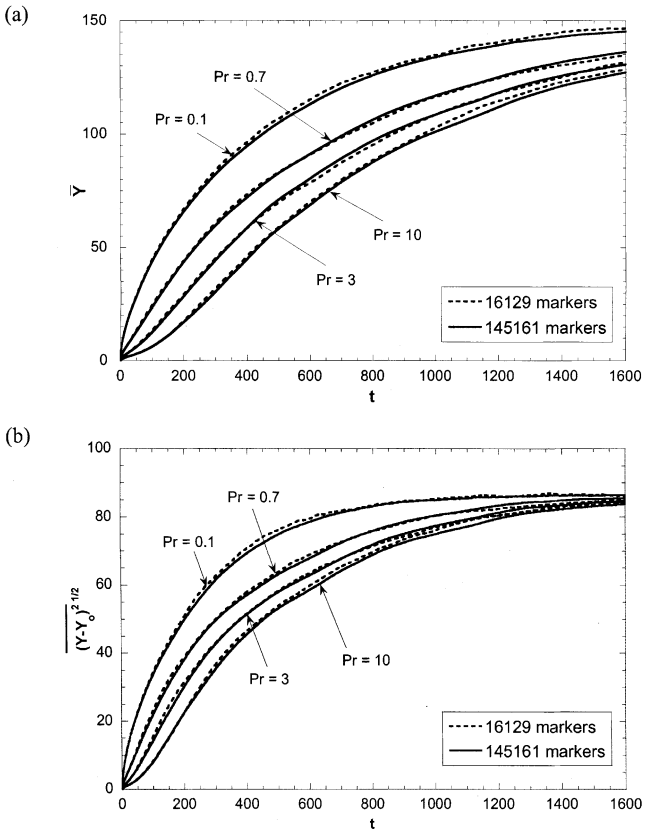

Figure 1. Comparison of results between runs with different number of markers.

(a) Mean marker position in the vertical direction, (b) root mean square of the marker position relative to the cloud centroid in the vertical direction.

troid will be at $y = h = 150$. Figure 1b presents a similar comparison for the standard deviation of the probability of the marker location with time in the y-direction. Using the data in Figures 1a and 1b, it is found that the average difference in the statistical behavior of runs with the same Pr and different number of markers is less than 1.5%. It can be concluded that the use of samples with on the order of 10^4 markers can provide accurate results for the generation of first-order statistics. One should consider a balance between the computational cost that is associated with the creation of large data sets and the acceptable accuracy of the results, when employing LST. Results for different sample sizes will be shown in other figures in this article, when the transport properties are presented.

In order to validate the numerical experiments, results from the DNS/LST method are compared with experimental data, which are available for low Prandtl or Schmidt number fluids. Papavassiliou (2002b) presented such comparisons for the cases of runs A and B (16,129 markers); here both data sets for 16,129 and for 145,161 markers are used. Poreh and Cermak (1964) measured the mean concentration profile downstream from a continuous line source of ammonia gas in a turbulent boundary layer of air. The Schmidt number of their system was 0.72, and the line source was located at the wall. Using similarity arguments, they argued that dimensionless mean concentration profiles are universal and they introduced the plume half-width, δ_y, as a length scale defined to be the distance from the wall at which the concentration, C, falls to half its maximum

$$\frac{C}{C_{\max}} = f(\xi)$$

where

$$\xi = \frac{y}{\delta_y} \quad \text{and} \quad f(1) = 0.5 \tag{5}$$

Similar experiments were performed by Fackrell and Robins (1982), who measured concentration fluctuations and turbulent fluxes for a passive plume from a ground-level source in a turbulent boundary layer. The source gas consisted of a mixture of propane and helium, the former being used as a trace gas for concentration measurements. By using the plume half-width as a length scale, they proposed the following empirical relation

$$C = C_{\max} \exp\left\{ -0.693 \cdot \left(\frac{y}{\delta_y} \right)^s \right\} \tag{6}$$

where $s = 1.5$ gives the best fit to obtained experimental data.

Both experiments are compared with the results of the simulation herein. Calculated scalar concentration in the direction perpendicular to the wall, normalized with the maximum concentration, according to Eq. 5, agrees well with Poreh and Cermak's experiments for mass transfer at low Sc. Similarly, results from the DNS/LST method, fitted according to Eq. 6, give $s = 1.52$, which is very close to the value proposed by Fackrell and Robins ($s = 1.5$). Figure 2 shows the comparison between the experimental measurements and the numerical results for $Pr = 0.7$. This figure also illustrates the good agreement between LST experiments for the different number of heat markers.

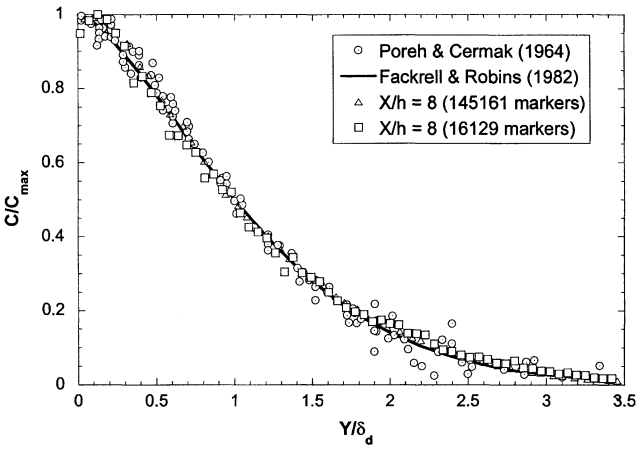

Figure 2. Results for $Pr = 0.7$ at $x = 8h$.

Comparison with experimental measurements by Poreh and Cermak (1964) and by Fackrell and Robins (1982).

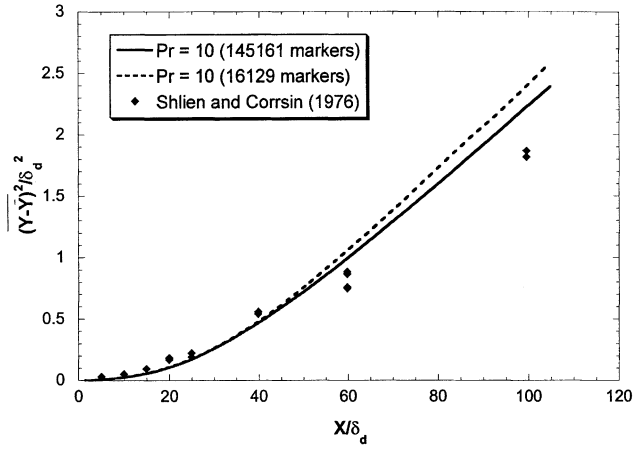

Figure 3. Comparison of LST results for turbulent dispersion downstream from a source with measurements by Shlien and Corrsin (1976) in a turbulent boundary layer.

Next, a comparison is done with the experiments of Shlien and Corrsin (1976), in which dispersion was measured in a turbulent boundary layer in a wind tunnel downstream of a heated wire located at the wall. Heat was supplied to the wire at a constant rate, so that their case is equivalent to the calculation of P_2 profiles using LST. They scaled the distance from the wall and the distance downstream from the source with the displacement thickness of the turbulent boundary layer, δ_d. In order to calculate the appropriate length scale for the channel flow DNS, it is assumed that the mean center-line velocity of the channel can be used in place of the free-stream velocity for the calculation of the momentum boundary layer. The calculated value for the DNS is $\delta_d = 23.2$. Also, for comparison with measurements, a plume for fluid with the same Pecklet number ($Pe = Re \cdot Pr$) is used, which corresponds to $Pr = 10$. Particle dispersion can be expressed with $\overline{(Y-\bar{Y})^2}$, where Y is the displacement in the direction perpendicular to the wall and $\bar{Y}$ is the mean marker displacement. Figure 3 shows the comparison between calculated turbulent dispersion downstream from the source and the experimental measurements. It appears that up to $x/\delta_d = 60$, there is agreement between Shlien and Corrsin's data and the simulation results. Given that Shlien and Corrsin investigated the physical problem of a developing boundary layer, and that the LST results are for a fully developed channel flow, the discrepancy between the results from these particular experiments should be expected to appear more at distances farther from the source, as seen in Figure 3.

Another comparison with the experiments of Fackrell and Robins (1982) is made for the measurements of turbulent scalar fluxes. The turbulent heat flux, $\overline{v\theta}$, normalized with the friction velocity u^* and the temperature at the wall T_w, can be found from the expression for the total heat flux in a dimensionless form

$$\frac{\overline{v\theta}}{u^* T_w} = \frac{1}{T_w^+}\left(1 - \frac{y^+}{h^+}\right) - \frac{1}{T_w^+ Pr}\left(\frac{d\overline{T^+}}{dy^+}\right) \qquad (7)$$

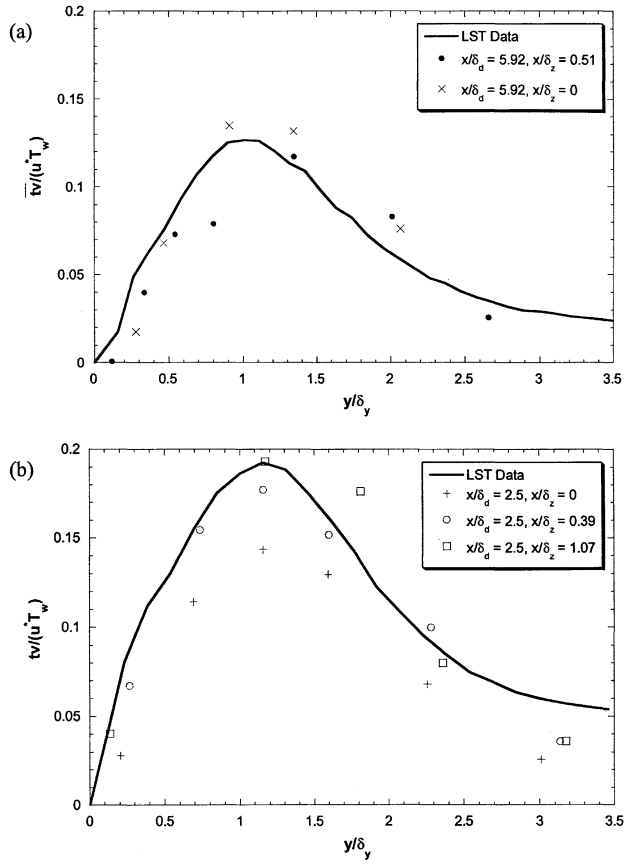

Figure 4. Comparison of the LST results for turbulent heat flux with measurements by Fackrell and Robins (1982).

(a) $x/\delta_d = 2.5$, (b) $x/\delta_d = 5.92$.

where v and θ are the fluctuating components of the velocity and temperature normal to the wall, and T^+ is the dimensionless mean temperature. Figures 4a and 4b show experimental results for the turbulent concentration flux $\overline{vc}$ at two different locations downstream from the source and the LST results obtained using Eq. 7. It should be noted that the laboratory experiments were performed for a single continuous point source and for different lateral locations, z/δ_z, where δ_z is the lateral half-plume width. Results for the line source, as in our case, basically represent the average value of the turbulent fluxes for different spanwise locations, z/δ_z. Taking this into account, it can be seen that the agreement between the LST results and the experimental measurements is good.

Batchelor's Lagrangian similarity theory

Batchelor (1964) presented the idea of applying similarity to dispersion in a turbulent shear flow. He assumed similarity of a form such that the statistical properties of the Lagrangian velocity within the constant stress region depends only on the friction velocity u^* and time, resulting in

$$\bar{V} \equiv \frac{d\bar{Y}}{dt} = bu^* \qquad (8)$$

where b is a universal constant. He also assumed that a constant c exists such that the mean Lagrangian velocity in the streamwise direction equals the Eulerian velocity located at $c\overline{Y}$, that is

$$\frac{d\overline{X}}{dt} = \left[\overline{U}(y)\right]_{y=c\overline{Y}} = \frac{u^*}{\kappa}\ln\frac{c\overline{Y}}{y_o} \tag{9}$$

where $\overline{X}$ is the mean downstream particle displacement, y_o is the length characterizing the wall roughness, and κ is Von Karman's constant ($\kappa = 0.41$). By combining Eqs. 8 and 9 and integrating, Batchelor obtained

$$\overline{X} = \frac{1}{b\kappa}\left[\overline{Y}\ln\left(\frac{c\overline{Y}}{y_o}\right) - \overline{Y} + A\right] \tag{10}$$

where A is the constant of integration that depends on the particle release position from the wall. Batchelor's similarity theory is compared with numerical calculations from the DNS/LST method in Table 2 as follows: the mean particle displacement in the streamwise and spanwise directions is calculated for the puffs for different Prandtl number fluids, and subsequently, Batchelor's Eq. 10 is used in order to estimate the universal constant b as a function of Pr. The calculated values for constants b and c are given in Table 2. It can be seen that for $Pr \le 10$, the value of the constant b agrees closely with Batchelor's estimation ($b \approx 0.2$). However, it can be seen that Batchelor's constants depend on Pr. As Pr increases, the cloud of markers stays in the viscous wall layer longer (Papavassiliou, 2002a), which affects the development of $\overline{X}$ with time. Batchelor's theory assumed that the whole cloud of markers is in the constant stress region, which is true only for low-Pr markers. It should be noted here that our values are calculated based on data for the development of a cloud of markers emitted instantaneously form a line source (a puff of markers), while previous measurements (Poreh and Cermak, 1964; Shlien and Corrsin, 1976) used data from a continuous line source at the wall (a plume of markers). Referring to the original derivation of Batchelor, it is evident that Eqs. 8 and 9 hold for a puff, and, therefore, Eq. 10 should be used to fit data from a puff of markers. Experimentally, however, it is very difficult to obtain time and space results from instantaneous line sources, while the present computational method provides the opportunity to calculate the constants in Eq. 10 using the proper data set.

Prandtl number effects on transport properties

Based on Taylor's analysis, Shlien and Corrsin (1976) defined a turbulent diffusivity as

$$D_t = U_\infty \frac{\partial}{\partial x}\left[\frac{1}{2}\overline{(Y - Y_o)^2}\right] \tag{11}$$

where U_∞ is the free-stream velocity and Y_o the position of the source. Equation 11 represents total diffusivity when molecular diffusivity effects are neglected. In the LST context, the turbulent diffusivity can be calculated by subtracting the contribution due to molecular diffusivity from the total diffusivity. Furthermore, since we can calculate the mean plume displacement in the direction normal to the wall, we can use the mean velocity at that location instead of the mean center-line velocity, in order to obtain more accurate calculations of the turbulent diffusivity in the near wall region. Thus, the turbulent diffusivity can be expressed as

$$D_t = U_{(y=\overline{Y})}\frac{\partial}{\partial x}\left[\frac{1}{2}\overline{(Y - Y_o)^2}\right] - \frac{1}{Pr} \tag{12}$$

The turbulent Prandtl number, Pr_t, can then be defined in terms of the eddy viscosity, E_v, as

$$Pr_t = \frac{E_v}{D_t} \tag{13}$$

In order to obtain an accurate estimation of Pr_t, the turbulent (eddy) viscosity is also calculated at the location of the mean cloud centroid, $\overline{Y}$ (which depends on x), instead of using an average (bulk) value across the channel. Equations 12 and 13 are used in order to examine the influence of molecular Pr on the turbulent diffusivity and on Pr_t. Figures 5a and 5b show changes in D_t downstream from the source for two different ranges of Pr. It can be seen that for higher Pr, at short distances from the source, D_t is close to zero, since the plume is mostly in the viscous wall layer and the markers move only due to molecular diffusion. At higher x, turbulent diffusion starts to dominate the dispersion of the plume and D_t rapidly increases. At one point D_t exhibits a maximum and finally starts to decrease due to the effects of the upper wall of the channel. It also can be seen that the molecular effect is important up to approximately $x = 8{,}000$ (which is $x/h \approx 55$), and from that point on all curves follow nearly the same descending trend. The $Pr = 2{,}400$ curve separates the medium-low from the medium-high Pr curves in the region where molecular effects are important. Eventually, markers are uniformly distributed in the channel confined between two walls, and the function $\overline{(Y - Y_o)^2}$ in Eq. 12 reaches a constant value. As a consequence, the first term on the right-hand side of the equation becomes zero, which implies that $D_t < 0$, since molecular diffusivity is positive. This result means that the definition of eddy diffusivity in the region of a fully developed plume is not appropriate. Such nonphysical values for eddy quantities (that is, eddy viscosity) have been known to exist in cases where the maximum of the mean velocity profile (the zero in the velocity gradient) and the zero in the total shear stress do not coincide. Churchill (1996) dis-

Table 2. Batchelor's Constants b and c for Differential Prandtl Number Fluids

Pr	b	c
0.1	0.12	0.21
0.7	0.12	0.45
1	0.12	0.53
3	0.14	1.07
10	0.19	4.95
100	0.3	300

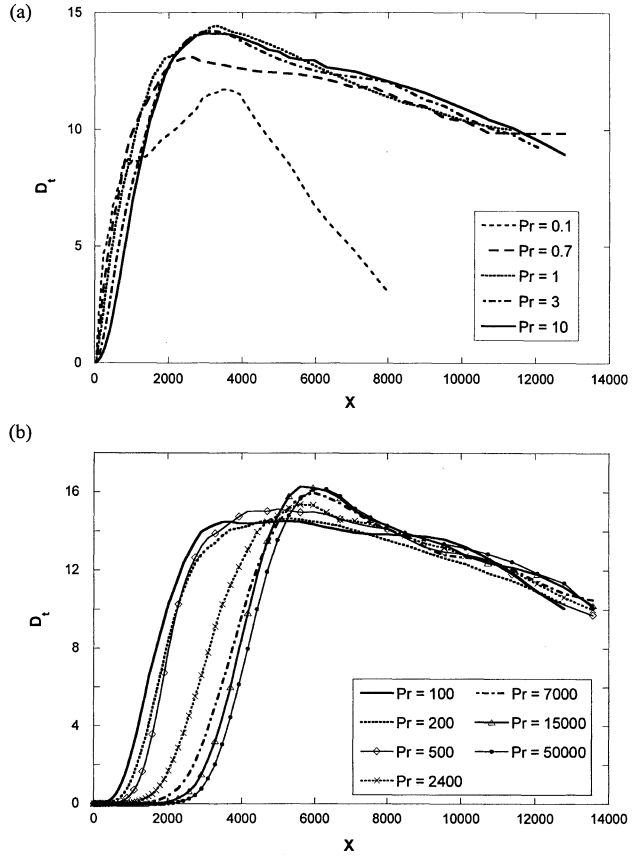

Figure 5. Turbulent diffusivity for the plume in the downstream direction as a function of *Pr*.

(a) Low-*Pr* runs ($Pr \leq 10$), (b) high-*Pr* runs ($Pr \geq 100$).

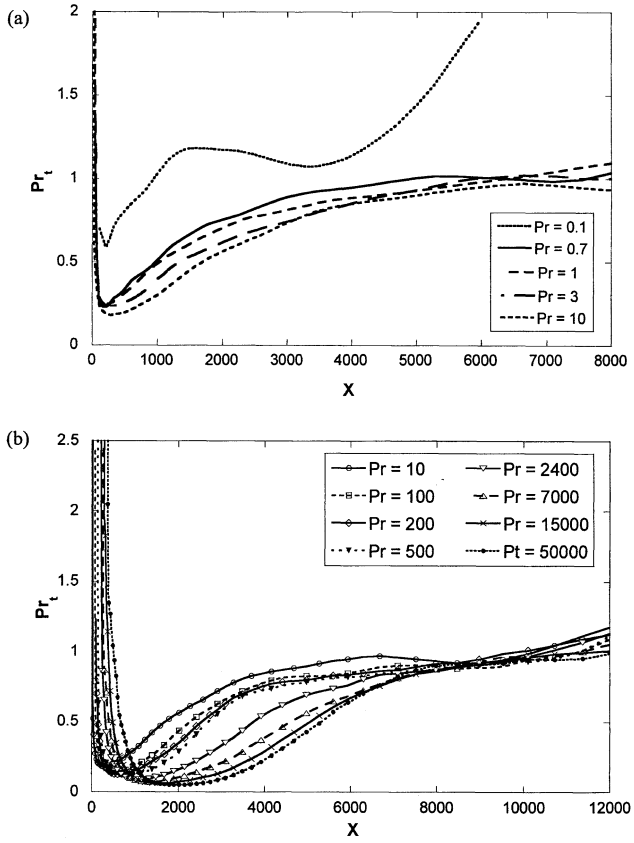

Figure 6. Turbulent Prandtl number for the plume in the downstream direction as a function of *Pr*.

(a) Low-*Pr* runs ($Pr \leq 10$), (b) medium- and high-*Pr* runs ($Pr \geq 10$).

cussed this issue for the case of asymmetric flows, such as turbulent flow in an annulus and turbulent flow in a channel with a smooth and a rough wall.

Figures 6a and 6b present the turbulent Prandtl number downstream from the source for low and high *Pr* runs, respectively. In accordance to Eqs. 12 and 13, at short distances downstream from the source, Pr_t is very high, since the turbulent diffusivity is equal or close to zero. This corresponds to the region where molecular diffusion dominates the dispersion. In the Eulerian sense, the eddy viscosity is much larger than the eddy diffusivity in the viscous wall sublayer, and in the Lagrangian sense, the markers that compose the plume immediately downstream from the source are in their respective positions mostly due to molecular diffusion and not due to turbulence. Other evidence that E_υ and D_t have different limiting behavior in the viscous wall sublayer can be found from the DNS results obtained by Na and Hanratty (2000) for the case where isothermal boundary conditions were imposed on the channel walls. They have found that the limiting behavior for the eddy viscosity is $E_\upsilon = 0.00079y^3$, while the preexponential factor in the limiting expression for the eddy diffusivity decreases with the increase of *Pr*, and it is $D_t = 0.00073y^3$ and $D_t = 0.00053y^3$ for the $Pr = 1$ and $Pr = 10$, respectively. This also implies that we may expect a $Pr_t > 1$ close to the wall that will become higher at higher molecular *Pr*. Furthermore, the distance in the direction downstream from the line source where Pr_t is higher than the one that is longer for higher *Pr*. After reaching a minimum, Pr_t slowly increases in the transitional region where both molecular diffusion and turbulent convection affect the dispersion. In the Lagrangian sense, the markers reach their locations due to both turbulence and molecular diffusion. In both these regions strong *Pr* influence on Pr_t can be observed. At some point farther downstream, uniformly distributed markers are only under the influence of turbulent convection and there is no clear distinction between curves for different values of *Pr*. It should also be noted that for a wide span of downstream distances, the turbulent Prandtl number has values that are close to the Reynolds analogy ($Pr_t = 1$).

Herein the physical meaning of the eddy diffusivity is considered to be the ratio of the contribution to the heat flux due to the turbulence fluctuations over the contribution to the heat flux due to molecular means. The physical meaning of the turbulent Prandtl number is considered to be the ratio of the transport of momentum due to turbulent fluctuations divided by the transport of heat or mass due to turbulent fluctuations. In this respect, the preceding discussion of the eddy diffusivity and of Pr_t is the Lagrangian analog for the case of a plume of the Eulerian interpretation of the eddy diffusivity and of Pr_t, which was presented recently by Churchill (2002). In that work, Churchill disassociated the

physical meaning of eddy viscosity and eddy diffusivity from their original diffusional definition and interpreted them as the ratio of the momentum or energy flux due to turbulence to that due to molecular means. In the Lagrangian sense, the physical meaning of the eddy diffusivity is to consider the percentage of new markers that arrive at a particular location in the flow field due to turbulence effects, that is, the ratio of the markers that arrive at a location after having left the viscous wall layer, and after being dispersed in the flow field due to velocity eddies, to the markers that arrive at that location as a result of molecular motion (those that arrive from the wall without spending time in the outer region or those that arrive from the viscous wall region of the other wall). Therefore, the eddy diffusivity is expected to increase within the plume as the distance downstream from the line source increases, because the percentage of markers that arrive at locations farther away from the source are more likely to wander outside the viscous wall sublayer (as evidenced by the increase in the plume width). At some point, the effect of the top wall of the channel manifests itself. A number of markers start entering the viscous wall sublayer associated with the top wall, so that the eddy thermal diffusivity begins to decrease. At the same time, as the distance from the source increases even farther, the distribution of markers across the plume becomes more uniform, resulting in a decrease in the total heat flux across the channel (both due to turbulence and due to molecular effects). Markers that arrive at those locations do not arrive there because turbulence disperses them; turbulence does not really add to the dispersion of these markers. Eventually there is no heat flux across the channel (that is, the markers are uniformly distributed across the channel), and, thus, no meaning to the definition of a heat flux due to turbulence motion.

In order to determine the effect of Pr on Pr_t, values for the downstream distance x, where $Pr_t = 0.5$, have been correlated with Pr. There are two intercepts between $Pr_t = 0.5$ and the curves on Figure 6b, which can be used to quantify the different Pr dependence in the zone where molecular diffusion dominates the dispersion and in the transitional zone. In the first zone, a Pr number dependence is observed for high values of Pr ($2{,}400 \le Pr \le 50{,}000$), where x at which $Pr_t = 0.5$ can be approximated with $48.94 \cdot Pr^{0.25}$. In the second zone, values for this downstream distance, x, can be correlated with $1{,}088 \cdot Pr^{0.16}$ for all Pr. By using these correlations, an appropriate functional relation between Pr_t and Pr can be found. Figures 7a–7c show Pr_t vs. distance in the downstream direction, where all curves nearly collapse on one. Hence, the following scaling is proposed

Zone I: $Pr_t \cong f(Pr^{-1/4})$ for $2{,}400 \le Pr \le 50{,}000$

Zone II: $Pr_t \cong f(Pr^{-1/6})$ for all Pr

Zone III: $Pr_t \neq f(Pr)$ for all Pr

The observation of these three plume-development zones is related to the fact that the plume is synthesized by the behavior of a puff of markers. It has been found (Papavassiliou, 2002a) that the behavior of the cloud that results from an instantaneous line source (puff) develops in three stages: Zone I, in which molecular diffusion dominates dispersion; Zone II, which is a transition zone; and Zone III, in which

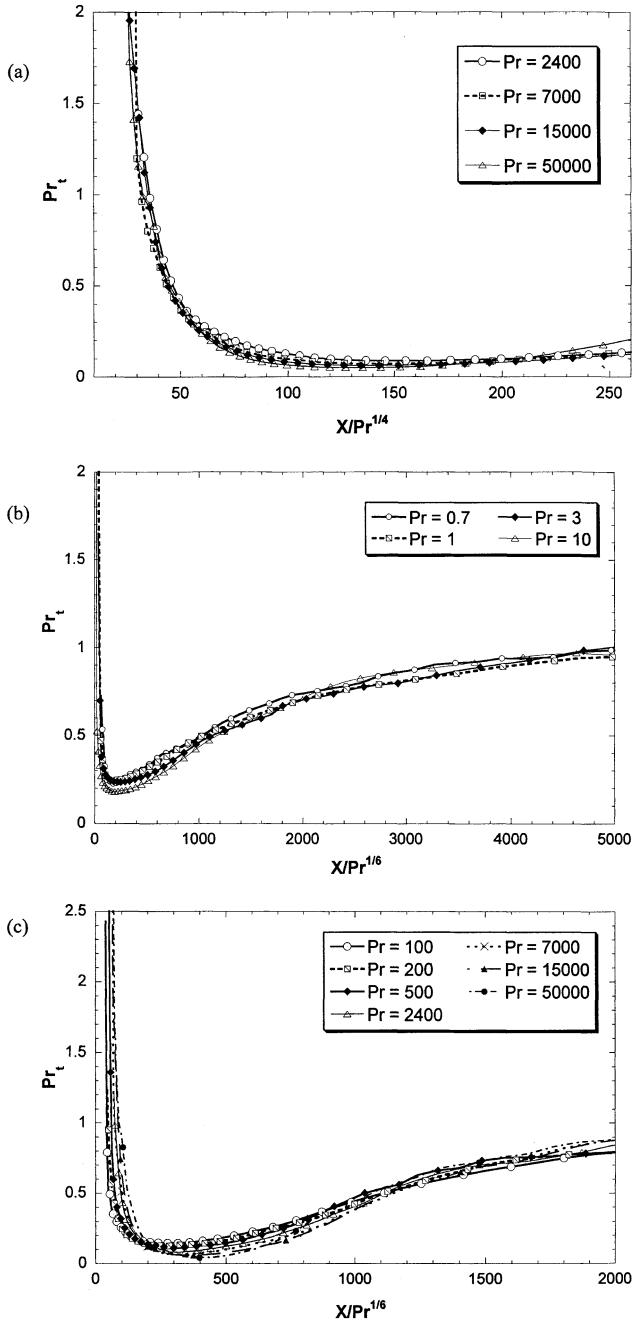

Figure 7. Turbulent Prandtl number vs. scaled downstream distance x.

(a) High-Pr runs ($2{,}400 \le Pr < 50{,}000$), Zone I; (b) low-$Pr$ runs ($0.7 \le Pr \le 10$), Zone II; (c) medium- and high-Pr runs ($100 \le Pr < 50{,}000$), Zone II.

turbulent convection dominates dispersion. The extent of Zones I and II depends on the Pr; it becomes longer as the Pr increases. In Zone I the cloud markers stay close together and the cloud grows similarly to a balloon that starts to expand within the viscous wall layer. In the transition zone, some markers leak out of the balloon formation and large eddies sweep them away from the viscous wall region, forming a secondary cloud. Therefore, in this zone there exist two

distinguishable clouds, the first of which is the original cloud that moves slowly within the viscous wall region as it leaks markers, and the second is the cloud formed by the leaked markers, which moves much faster due to the higher mean streamwise velocity in the region away from the channel walls. The higher the *Pr*, the smaller the molecular jumps and the more difficult it is for the markers to leak out of the original cloud (the one moving within the viscous sublayer) to the outer region, and the more extended Zone II of the puff evolution becomes. The plume is formed by puffs at different stages of development. In this sense, close to the continuous line source, the plume is formed by puffs that are in Zone I of development, a little farther downstream by puffs that are in Zone I and in Zone II, and even farther away by puffs in Zone III. Since the extent of these first two zones is *Pr* dependent, it is expected to observe *Pr* dependence on the turbulent transport properties, as well as the temperature profile, close to the source.

The preceding Lagrangian description of the evolution of a plume can be taken a step further to interpret the dependence of turbulent transport properties (such as the eddy conductivity and the turbulent Prandtl number) on molecular properties (that is, the *Pr*) for the case of transport from the wall, contrary to isotropic turbulence. When a wall is present, turbulence becomes more important for the movement of the markers, and, therefore, eddy conductivity becomes larger, when the markers leak out of puffs that are in Zone I of puff development. However, in order for the leaking process to happen, eddies that have velocity fluctuations in the vertical direction must assist the Brownian motion to move markers out of the viscous wall sublayer. The higher the *Pr*, the smaller the random molecular jumps in the vertical direction (see the relation between the standard deviation of the distribution of the molecular jumps and the *Pr* in the third section) and the harder it is for turbulence eddies to sweep markers away from the wall. In fact, the higher the *Pr*, the larger the size and intensity (that is, the size of the fluctuating velocity) of the eddies that are able to contribute to the transport of markers away from the wall. In other words, only a part of the turbulence spectrum contributes to turbulent transport close to the wall (the larger wavelengths and smaller wavenumbers), and the part of it that contributes is a function of *Pr*. As the *Pr* increases, a larger part of the turbulence spectrum is not contributing to turbulent transport. This is the Lagrangian interpretation of the "filtering" effect that the wall exhibits on the turbulence spectrum that contributes to mass transfer. Evidence of this filtering effect has been found both experimentally (Campbell and Hanratty, 1983) and computationally using Eulerian DNS (Na and Hanratty, 2000). In fact, the filtering effect has been used to determine the cutoff point of the turbulence spectrum in the context of large eddy simulation for flows with *Pr* as high as 200 (Calmet and Magnaudet, 1997).

Prediction of the mean temperature profile as a function of Pr

The first step is to evaluate the decay of the ground-level concentration, T_{max}, from the continuous source in the streamwise direction. The calculated values normalized with the source strength (the total number of markers released per time step) for different values of *Pr* are presented in Figure 8. Two zones of plume development with different rates of decay of T_{max} can be distinguished, as were observed by Papavassiliou (2002b) using data only from runs A and B. The change in the slope of the line, far from the source location, becomes more evident for higher *Pr*. If we assume, based on Batchelor's (1964) prediction that $T_{max} \sim 1/x$, that the first zone is described by a power function, $A \cdot (Pr/x)^a$, and the second one by a function, $B \cdot (Pr/x)^b$, then the normalized temperature, T_{max}, at any location x downstream from the source, can be determined from the following expression

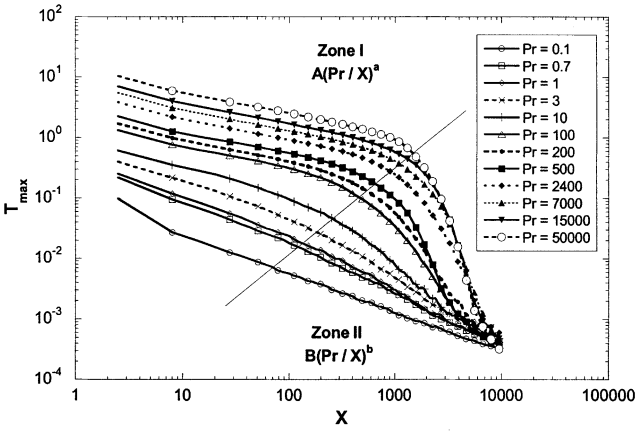

Figure 8. Normalized ground-level temperature downstream from a continuous line source.

$$T_{max} = \frac{A \cdot B \cdot \left(\frac{Pr}{x}\right)^{(a+b)}}{A \cdot \left(\frac{Pr}{x}\right)^{a} + B \cdot \left(\frac{Pr}{x}\right)^{b}} \tag{14}$$

Table 3 presents the calculated values of the coefficients in Eq. 14, for different *Pr*. Since the values for coefficients *A*, *B*, *a*, and *b* follow a specific trend for a specific *Pr* range, the functional relations between the coefficients and *Pr* can be obtained. Table 4 presents the proposed functions and their accuracy.

Table 3. Coefficients for the Ground-Level Temperature T_{max} vs. x Correlation for the Two Zones of Plume Development (Eq. 14)

	Zone I		Zone II		
Pr	A	*a*	B	*b*	R^2
0.1	0.432	0.62	43.4	0.87	1.000
0.7	0.515	0.65	43.4	1.18	0.999
1	0.438	0.59	43.4	1.30	1.000
3	0.371	0.52	43.4	1.54	1.000
10	0.332	0.45	43.4	1.84	0.999
100	0.309	0.39	14.9	2.56	0.998
200	0.296	0.40	6.72	2.74	0.998
500	0.291	0.38	1.26	3.03	0.996
2,400	0.263	0.39	4.29×10^{-2}	3.42	0.997
7,000	0.187	0.38	2.76×10^{-4}	3.31	0.996
15,000	0.246	0.38	1.37×10^{-4}	3.90	0.996
50,000	0.237	0.38	4.06×10^{-7}	4.30	0.996

Table 4. Correlation for the Coefficients in Eq. 14 as a Function of *Pr*

Coefficient	*Pr* No. Range	R^2
$A = 0.459 * Pr^{-0.154}$	$0.1 \le Pr \le 10$	0.923
$A = 0.369 * Pr^{-0.042}$	$10 \le Pr \le 50{,}000$	0.990
$a = 0.5984 * Pr^{-0.1}$	$0.1 \le Pr \le 100$	0.956
$a = 0.385$	$100 \le Pr \le 50{,}000$	0.991
$B = 43.4$	$0.1 \le Pr \le 100$	1.00
$B = 1.86 * 10^7 * Pr^{-2.76}$	$100 \le Pr \le 50{,}000$	0.967
$b = 0.27 * \ln(Pr) + 1.319$	$0.1 \le Pr \le 50{,}000$	0.996

The two zones just described are related to the three zones of puff development: the first one is affected by puffs in their Zone I stage of development, and the second is affected by puffs in their Zone II stage of development. Zone III is manifested here by the collapse of $T_{\max}$ to a constant value for $x > 10{,}000$. The distance at which the transition from Zone I to Zone II occurs can be found as the intersection of the lines that define these two zones. Values of the transitional x are plotted as a function of *Pr* on a logarithmic scale (Figure 9). As indicated in the figure, the x_{tr} can be represented by

$$x_{tr} = 196.5 \cdot Pr^{0.23} \tag{15}$$

The next step is to determine the vertical temperature distribution as a function of $T_{\max}$ and *Pr*. It already has been discussed (Eq. 5) that the nondimensional concentration (or temperature) profile in the direction perpendicular to the wall can be expressed in terms of the lateral plume half-width δ_y. The growth of δ_y in the direction downstream from the source is presented in Figure 10 for a wide range of *Pr*. As *Pr* increases, the distance for which the majority of the plume is very close to the wall also increases, as expected. For example, for $2{,}400 \le Pr \le 50{,}000$ and up to $x = 5{,}000$, the vertical plume spread is negligible and the prediction is limited to only the prediction of the ground-level concentration. Distances where the plume starts to expand in the normal direction for different *Pr* can be determined from Figure 10. A comparison of the development of the plume is also made between the two sets of numerical experiments with a different number of heat markers. Figure 11 shows that the agreement for δ_y for 16,129 markers is quite good.

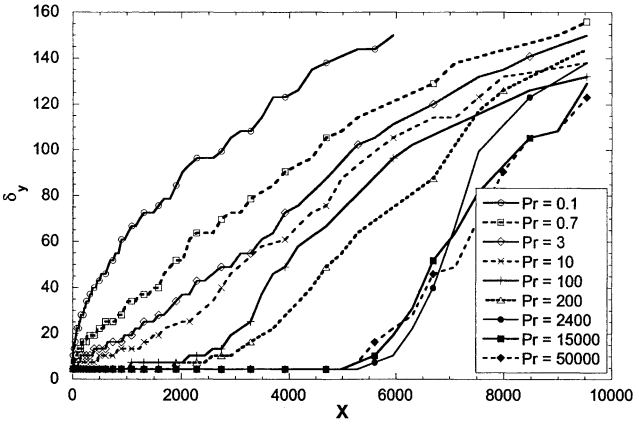

Figure 10. Half plume width downstream from a continuous line source.

Poreh and Hsu (1971) found experimentally for $Pr = 0.7$ that the variation of δ_y with distance x has a power-law dependence, so that $\delta_y \sim x^{0.8}$. Similarly, Fackrell and Robins (1981) proposed that $\delta_y \sim x^{0.75}$ for the same value of *Pr*. From the DNS/LST data, it is found that $\delta_y \sim x^{0.72}$, which is in good agreement with these experimental measurements. However, it appears that for higher values of *Pr*, the half plume width is a more complex function of x, and it cannot be easily implemented for the prediction of the mean concentration profile. Also, as pointed out by Shlien and Corrsin (1976), the use of $T_{\max}$ and δ_y as scaling parameters is an insensitive way to determine similarity, because such scaling forces two points on a monotonically decreasing curve to coincide (the $\xi = 0$ point and the $\xi = 1$ point). The development of the marker cloud does not need to scale with δ_y in the case of fully developed channel flow. Figures 12a–12c present the dimensionless concentration profile in the direction perpendicular to the wall as a function of *Pr*, using the channel half-height, h, as a length scale. It can be seen that

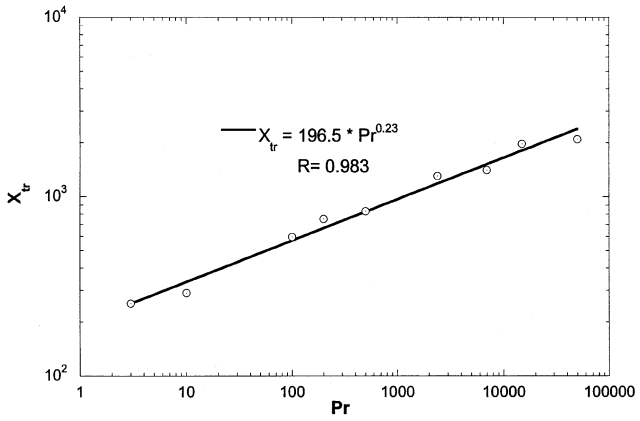

Figure 9. Distance x from a continuous line source at which transition from Zone I to Zone II occurs.

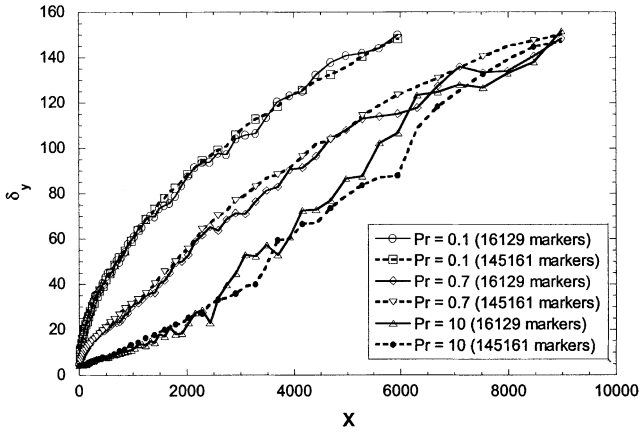

Figure 11. Half plume width: comparison between runs for different numbers of markers.

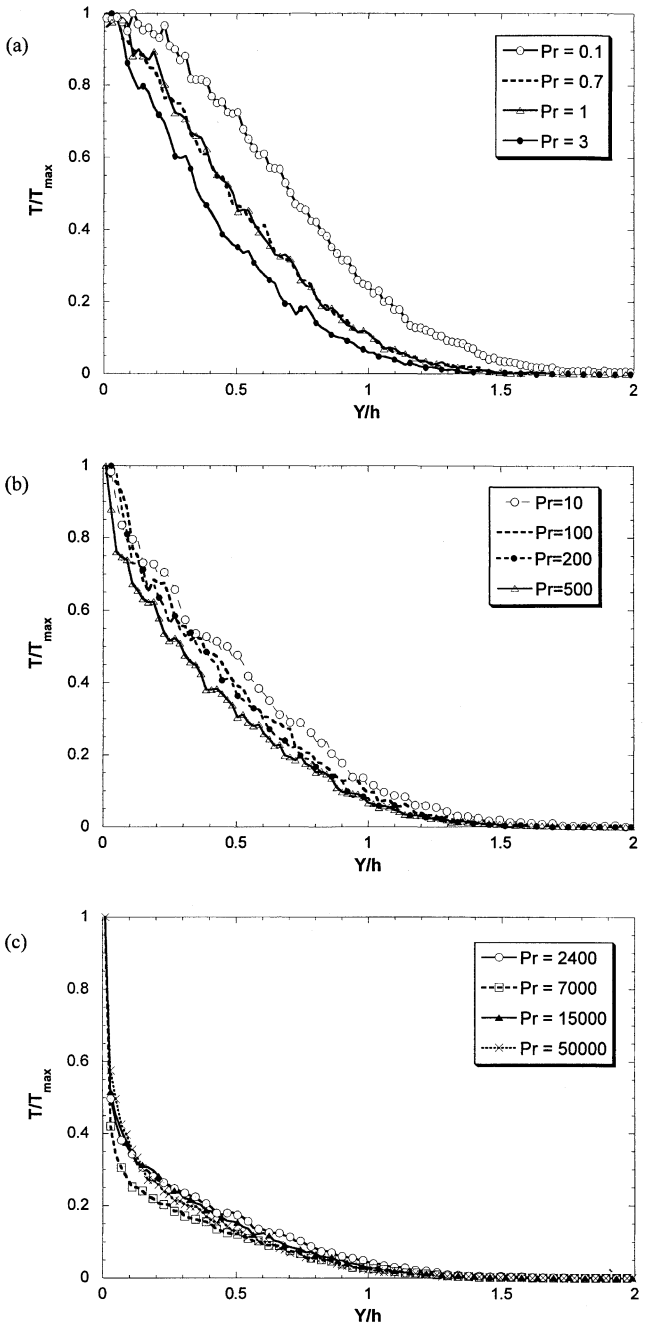

Figure 12. Dimensionless temperature profile in the vertical direction.

(a) Low-*Pr* runs ($Pr \le 3$) at $x/h = 20$; (b) medium- and high-*Pr* runs ($10 \le Pr \le 500$) at $x/h = 27$; (c) high-*Pr* runs ($500 \le Pr \le 50{,}000$) at $x/h = 33$.

for low values of *Pr* there is a strong *Pr* effect on the nondimensional concentration in the normal direction. For higher values of *Pr*, this dependence tends to decrease and lines for different values *Pr* almost fall one on top of the other. Also, *Pr* effects decrease downstream from the source.

Hence, three different ranges of *Pr*, where different approximations can be applied, are distinguished. The first one is the low-*Pr* region ($0.1 \le Pr \le 3$), where the plume behavior can be approximated with the following relations

$$\frac{T}{T_{\max}} = \exp\left[-114 \cdot \left(\frac{y}{h}\right)^{1.72} \left(\frac{h}{x}\right)^{1.25} Pr^{s_2}\right] \tag{16}$$

$$s_2 = -0.157 \cdot \ln(x) + 1.575 \tag{17}$$

It should be noted that the exponent for the dimensionless distance from the wall *y/h* is 1.72, which is very close to the value found experimentally when *y* is normalized with δ_y. Equations 16 and 17 are valid for the whole range of *x*, since for low *Pr* fluids the plume starts to expand in the normal direction at the source. The second region is for medium values of *Pr* ($10 \le Pr \le 500$), for which the following correlations are proposed

$$\frac{T}{T_{\max}} = \exp\left[-193 \cdot \left(\frac{y}{h}\right)^{s_1} \left(\frac{h}{x}\right)^{1.34}\right] \tag{18}$$

$$s_1 = 2 \cdot 10^{-4} \cdot x + 0.263 \tag{19}$$

Equations 18 and 19 are valid for $x > 2{,}000$. As mentioned before, for up to $x = 2{,}000$ the plume resides mostly in the viscous wall region and the vertical plume-spread is negligible. Finally, the third region is for very high values of *Pr* ($2{,}400 \le Pr \le 50{,}000$), which can be described by

$$\frac{T}{T_{\max}} = \exp\left[-2{,}340 \cdot \left(\frac{y}{h}\right)^{s_1} \left(\frac{h}{x}\right)^{1.89}\right] \tag{20}$$

$$s_1 = 2 \cdot 10^{-4} \cdot x - 0.618 \tag{21}$$

Equations 20 and 21 are valid for $x > 5{,}000$.

Figure 13 presents data and model predictions obtained by using Eqs. 16–21. A representative value of *Pr* is used within each of the three described regions. It can be seen that the approximations are quite reliable. It should be mentioned that one of the advantages of scaling with the channel half-height is that the model eventually can be applied for mean-temper-

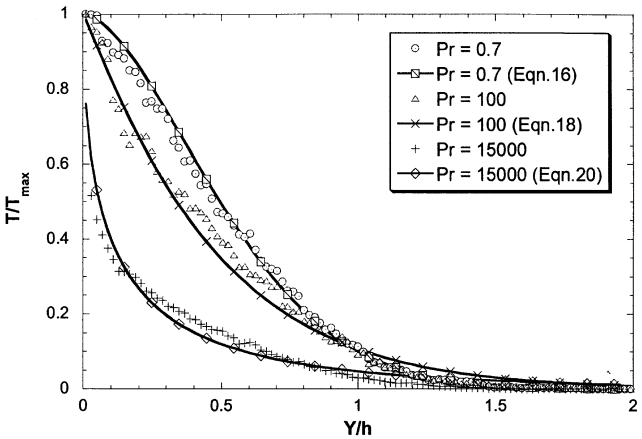

Figure 13. Comparison of Lagrangian simulations for the dimensionless temperature profile with fitted correlations.

ature predictions in a round tube, since h can simply be replaced with the radius of the tube according to an analogy by MacLeod (1951). By following the described procedure for predicting the ground-level temperature and the normal-temperature distribution, it is possible to obtain the mean-temperature profile for plumes for different values of Pr in the same channel. Predicted plume spreads were compared with data calculated with the LST, as shown in Figures 14a–14c for three Pr-number fluids.

Conclusions

Understanding the behavior of individual heat sources can lead to understanding the macroscopic turbulent heat transport mechanism. The challenge is to model and predict this behavior in time and space. A combined DNS/LST method is used in this work to simulate turbulent heat/mass transfer from a line source at the wall of a channel at different values of the Pr number. The numerical results agree well with experimental measurements in similar situations, allowing the

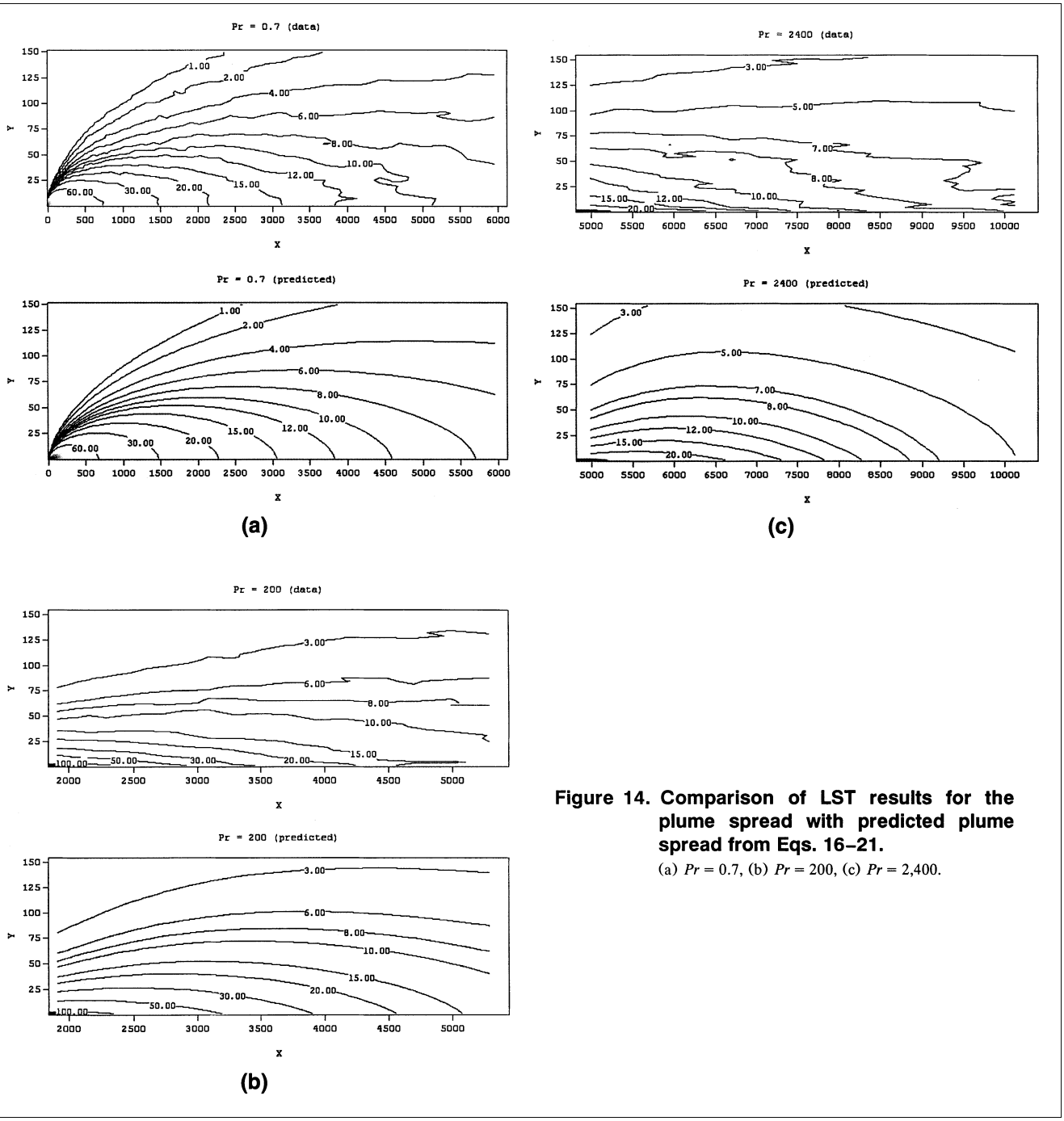

Figure 14. Comparison of LST results for the plume spread with predicted plume spread from Eqs. 16–21.

(a) $Pr = 0.7$, (b) $Pr = 200$, (c) $Pr = 2{,}400$.

calculation of the constants in Batchelor's Lagrangian similarity theory as a function of *Pr*. In the case of transport from the wall, it is shown that there is dependence on *Pr*, because markers released from the wall have to cross the viscous wall sublayer before entering the logarithmic region.

The development of a cloud of passive contaminants that results from a continuous line source located at the wall of the channel is studied. The turbulent Prandtl number exhibits three regions of development, which correspond directly to the three stages of development of a cloud that results from an instantaneous line source. The ground-level concentration exhibits two *Pr*-dependent regions of development, the first of which can be associated with Zone I of puff development, while the second can be associated with Zones II and III of puff development. Reduction of the plume behavior into the behavior of the puff leads to the Lagrangian interpretation of the dependence of turbulent transport properties on molecular properties in the case of transport from a wall. Different parts of the turbulence velocity spectrum contribute to turbulent transport from the wall, with the larger eddies contributing most to transport at higher *Pr* fluids. Transition from stage to stage is depicted. Furthermore, a model for the prediction of the temperature/concentration profile downstream from a continuous line source is developed. The model incorporates the effects of *Pr* and the stages of plume development. In addition to predicting plume behavior, the significance of such a model lies in the fact that a plume is the building block for the behavior of a heated plate, just as the behavior of a puff is the building block for the behavior of a plume. In other words, integration of the plume results in space will provide the behavior of a plate that is covered with an infinite number of continuous line sources located at the wall, which is the behavior of a heated plate. This way, LST can provide models for eddy diffusivity and heat-transport coefficients for the case of a heated channel wall.

The LST method has been used in this work to interpret Eulerian results and to calculate Eulerian transport properties. One of the next steps for LST will be the study of Reynolds number effects on turbulent transport, which have not been considered here. Experimental measurements for mass transfer (Shaw and Hanratty, 1977) indicate that a change in *Re* by a factor of 5 might not have an effect on the mass-transport coefficient. Another step will be the application of LST in round pipes, in order to evaluate the possibility of generalizing results for channels, as suggested by the MacLeod analogy.

Acknowledgments

The work was partially supported by the National Computational Science Alliance under CTS-990021N and utilized the NCSA HP/Convex Exemplar SPP-2000 and the NCSA SGI/CRAY Origin2000. The support of NSF under CTS-0209758 is gratefully acknowledged. Access to data from Tom Hanratty's laboratory at the University of Illinois is also gratefully acknowledged. We also acknowledge the insightful comments made by the anonymous referees that have led to the significant improvement of the manuscript.

Literature Cited

Batchelor, G. K., "Diffusion from Sources in a Turbulent Boundary Layer," *Arch. Mech. Stos.*, **3**, 661 (1964).

Calmet, I., and J. Magnaudet, "Large-Eddy Simulation of High-Schmidt Number Mass Transfer in a Turbulent Channel Flow," *Phys. Fluids*, **9**, 438 (1997).

Campbell, J. A., and T. J. Hanratty, "Turbulent Velocity Fluctuations that Control Mass Transfer to a Solid Boundary," *AIChE J.*, **29**, 215 (1983).

Cermak, J. E., "Lagrangian Similarity Hypothesis Applied to Diffusion in Turbulent Shear Flow," *J. Fluid Mech.*, **15**, 29 (1963).

Churchill, S. W., "A Critique of Predictive and Correlative Models for Turbulent Flow and Convection," *Ind. Eng. Chem. Res.*, **35**, 3122 (1996).

Churchill, S. W., "Critique of the Classical Algebraic Analogies Between Heat, Mass, and Momentum Transfer," *Ind. Eng. Chem. Res.*, **36**, 3866 (1997).

Churchill, S. W., "A Reinterpretation of the Turbulent Prandtl Number," *Ind. Eng. Chem. Res.*, **41**(25), 6393 (available on the web at http://pubs3.acs.org/acs/journals/doilookup?in_doi = 10.1021/ie011021k) (2002).

Eckelman, D. L., and T. J. Hanratty, "Interpretation of Measured Variations of the Eddy Conductivity," *Int. J. Heat Mass Transfer*, **15**, 2231 (1972).

Einstein, A., "Uber die von der molekular-kinetischen Theorie der Warme geforderte Bewegung von in ruhenden Flussigkeiten suspendierten Teilchen," *Ann. Phys.*, **17**, 549 (1905).

Fackrell, J. E., and A. G. Robins, "Concentration Fluctuations and Fluxes in Plumes from Point Sources in a Turbulent Boundary Layer," *J. Fluid Mech.*, **117**, 1 (1982).

Guenther, A., D. V. Papavassiliou, M. D. Warholic, and T. J. Hanratty, "Turbulent Flow in a Channel at Low Reynolds Number," *Exp. Fluids*, **25**, 503 (1998).

Hanratty, T. J., "Heat Transfer Through a Homogeneous Isotropic Turbulent Field," *AIChE J.*, **2**, 42 (1956).

Incropera, F. P., J. S. Kerby, D. F. Moffat, and S. Ramadhyani, "Convection Heat Transfer from Discrete Heat Sources in a Rectangular Channel," *Int. J. Heat Mass Transfer*, **29**, 1051 (1986).

Kasagi, N., and N. Shikazono, "Contribution of Direct Numerical Simulation to Understanding and Modeling Turbulent Transport," *Proc. R. Soc. London A*, **451**, 257 (1995).

Kasagi, N., Y. Tomita, and A. Kuroda, "Direct Numerical Simulation of Passive Scalar Field in a Turbulent Channel Flow," *Trans. ASME*, **114**, 598 (1992).

Kawamura, H., K. Ohsaka, H. Abe, and K. Yamamoto, "DNS of Turbulent Heat Transfer in Channel Flow with Low to Medium-High Prandtl Number Fluid," *Int. J. Heat Fluid Flow*, **19**, 482 (1998).

Kim, J., and P. Moin, "Transport of Passive Scalars in a Turbulent Channel Flow," *Turbulent Shear Flows*, J. C. Andre, J. Cousteix, F. Durst, B. E. Launder, F. W. Schmidt, and J. H. Whitelaw, eds., Vol. 6, Springer, Berlin, p. 85 (1989).

Kontomaris, K., T. J. Hanratty, and J. B. McLaughlin, "An Algorithm for Tracking Fluid Particles in a Spectral Simulation of Turbulent Channel Flow," *J. Comput. Phys.*, **103**, 231 (1993).

Lyons, S. L., T. J. Hanratty, and J. B. McLaughlin, "Direct Numerical Simulation of Passive Heat Transfer in a Turbulent Channel Flow," *Int. J. Heat Mass Transfer*, **34**, 1149 (1991a).

Lyons, S. L., T. J. Hanratty, and J. B. McLaughlin, "Large-Scale Computer Simulation of Fully Developed Turbulent Channel Flow with Heat Transfer," *Numer. Methods Fluids*, **13**, 999 (1991b).

MacLeod, A. L., "Liquid Turbulence in a Gas Absorption System," PhD Thesis, Carnegie Institute of Technology, Pittsburgh, PA (1951).

Mito, Y., and T. J. Hanratty, "Lagrangian Stochastic Simulation of Turbulent Dispersion of Heat Markers in a Channel Flow," *Int. J. Heat Mass Transfer* (2001).

Moin, P., and K. Mahesh, "Direct Numerical Simulation: A Tool in Turbulence Research," *Annu. Rev. Fluid Mech.*, **30**, 539 (1998).

Na, Y., and T. J. Hanratty, "Limiting Behavior of Turbulent Scalar Transport Close to a Wall," *Int. J. Heat Mass Transfer*, **43**, 1749 (2000).

Na, Y., D. V. Papavassiliou, and T. J. Hanratty, "Use of Direct Numerical Simulation to Study the Effect of Prandtl Number on Temperature Fields," *Int. J. Heat Fluid Flow*, **20**, 187 (1999).

Papavassiliou, D. V., "Scalar Dispersion from an Instantaneous Line Source at the Wall of a Turbulent Channel for Medium and High Prandtl Number Fluids," *Int. J. Heat Fluid Flow*, **23**, 161 (2002a).

Papavassiliou, D. V., "Turbulent Transport from Continuous Sources at the Wall of a Channel," *Int. J. Heat Mass Transfer*, **45**, 3571 (2002b).
Papavassiliou, D. V., and T. J. Hanratty, "The Use of Lagrangian Methods to Describe Turbulent Transport of Heat from the Wall," *Ind. Eng. Chem. Res.*, **34**, 3359 (1995).
Papavassiliou, D. V., and T. J. Hanratty, "Transport of a Passive Scalar in a Turbulent Channel Flow," *Int. J. Heat Mass Transfer*, **40**, 1303 (1997).
Ponoth, S. S., and J. B. McLaughlin, "Numerical Simulation of Mass Transfer for Bubbles in Water," *Chem. Eng. Sci.*, **55**, 1237 (2000).
Poreh, M., and J. E. Cermak, "Study of the Diffusion from a Line Source in Turbulent Boundary Layer," *Int. J. Heat Mass Transfer*, **7**, 1083 (1964).
Poreh, M., and K. S. Hsu, "Diffusion from a Line Source in Turbulent Boundary Layer," *Int. J. Heat Mass Transfer*, **14**, 1473 (1971).
Raupach, M. R., and B. J. Legg, "Turbulent Dispersion from an Elevated Line Source: Measurements of Wind Concentration Moments and Budgets," *J. Fluid Mech.*, **136**, 111 (1983).
Saffman, P. G., "On the Effect of the Molecular Diffusivity in Turbulent Diffusion," *J. Fluid Mech.*, **8**, 273 (1960).
Shaw, D. A., and T. J. Hanratty, "Turbulent Mass Transfer Rates to a Wall for Large Schmidt Numbers," *AIChE J.*, **23**, 28 (1977).
Shlien, D. J., and S. Corrsin, "Dispersion Measurements in a Turbulent Boundary Layer," *Int. J. Heat Mass Transfer*, **19**, 285 (1976).
Taylor, G. I., "Diffusion with Continuous Movements," *Proc. London Math. Soc.*, **24A**, 196 (1921).
Tennekes, H., and J. L. Lumley, *A First Course in Turbulence*, MIT Press, Boston, p. 96 (1972).
Tiselj, I., E. Pogrebnyak, L. Changfeng, A. Mosyak, and G. Hetsroni, "Effect of Wall Boundary Condition on Scalar Transfer in a Fully Developed Turbulent Flume," *Phys. Fluids*," **13**, 1028 (2001).

Manuscript received Dec. 4, 2001, and revision received Dec. 2, 2002.